Journal of Electrical and Computer Engineering Innovations
(JECEI)
Journal homepage: http://www.jecei.sru.ac.ir

Research paper

PAPR Reduction in OFDM UOWC System Employing Repetitive Clipping and Filtering (RCF) Method

B. Noursabbaghi, G. Baghersalimi*, A. Pouralizadeh, O. Mohammadian

Department of Electrical Engineering, University of Guilan, Rasht, Iran.

Article Info

Article History:
Received 01 August 2022
Reviewed 07 September 2022
Revised 07 October 2022
Accepted 03 December 2022

Keywords:
OFDM
UOWC
PAPR
RCF method

*Corresponding Author's Email Address: *bsalimi@guilan.ac.ir*

Abstract

Background and Objectives: High peak-to-average power ratio (PAPR) in Orthogonal Frequency Division Multiplexing (OFDM)-based Underwater Optical Wireless Communication (UOWC) systems is one main reason for out-of-band power and in-band distortion, leading to the degradation of system performance. Therefore, different approaches have been proposed, implemented, and examined for reducing the high PAPR of OFDM signals in such systems.

Methods: In this research, the performance of an OFDM-based UOWC system is investigated by employing the Repetitive Clipping and Filtering (RCF) technique in clear open ocean water. The Monte Carlo Modeling of Light (MCML) approach with the Henyey-Greenstein (HG) model of the scattering phase function is used to simulate the UOWC channel.

Results: The CCDF performance of the proposed system with the RCF method for various CR values is investigated. Also, the proposed system performance is examined in terms of bit error rate (BER) and error vector magnitude (EVM) at two different depths for link lengths of 1 m and 5 m.

Conclusion: The results show that the system performance is limited by increasing the link length, the number of subcarriers, and depth. Also, it is shown that the RCF method significantly leads to a reduction of the PAPR in the DCO-OFDM UWOC system and improves BER performance up to 10 dB.

Introduction

Recently, ocean exploration has attracted researchers' attention due to developments in military, industry, and scientific issues. Some of the most important applications of underwater wireless communications (UWC) include oceanography study, underwater surveillance, seafloor exploration, and monitoring, underwater oil pipe inspection, remotely operated vehicles (ROV), and sensor networks [1]-[5]. Although the dominant communications schemes used in underwater are still based mainly on the wireless technologies of radio frequency (RF) and acoustic (sonar), they suffer from low transmission data rate, limited bandwidth, high latency, and high attenuation which need to be addressed [6], [7].

One promising alternative complementary technology to aforementioned traditional schemes is optical waves. The underwater optical communications (UOWC) offer high speed (i.e., > 200 Mbps over a transmission range of up to 100 m), low attenuation (at the blue-green light wavelength of 450-550 nm), low latency, reliable and secure communication link which have become very attractive in recent years. However, UOWC link performance is affected by temperature fluctuations, scattering, dispersion, and beam steering leading to shorter transmission distance compared with other communication schemes [8].

Blue light-emitting diodes (LEDs) with phosphor coating are commonly used as a transmitter (Tx) in the UOWC systems which offer a long lifetime, energy efficiency, uniform illumination, and also simple fabrication with low cost. However, due to the slow response of phosphor, these LEDs have limited bandwidth (typically a few MHz). Moreover, white LEDs are the major source of nonlinearity in OWC systems which in turn causes signal distortion and intersymbol interference (ISI) [8], [9]. Some common solutions to mitigate these limitations are to employ multiple input-multiple output (MIMO) schemes, various equalization methods, and advanced modulation techniques [9], [10].

The simplest modulation scheme used in the UOWC systems is on-off keying (OOK), but it is not suitable for high data rate transmission due to its low spectral efficiency [10], [11]. As a result, there has been increasing interest in utilizing multi-carrier modulations such as orthogonal frequency division multiplexing (OFDM). The combination of OFDM with high-order quadrature amplitude modulation (QAM) can achieve higher data rate, higher spectral efficiency, simple one-tap equalization as well as inherent resistance to the ISI [12]. Two commonly OFDM schemes used in optical communications are asymmetrically clipped optical OFDM (ACO-OFDM) and DC-biased optical OFDM (DCO-OFDM). In this work, we use DCO-OFDM due to its higher spectral efficiency [13].

In [11] the authors evaluated the impact of different modulation orders of the QAM scheme in the OFDM-UOWC system. It was shown for a 2-m underwater channel that the best achievable bit rates are 161.36 Mb/s using 16-QAM at a BER of 2.5×10^{-3}, 156.31 Mb/s using 32-QAM at a BER of 7.42×10^{-4}, and 127.07 Mb/s using 64-QAM at a BER of 3.17×10^{-3}, respectively. In our previous work [14], the performance of an OFDM UOWC link for different depths was investigated in the clear open ocean. Results confirmed that the system BER performance degraded from 5.25×10^{-6} to 1.21×10^{-2} by increasing depth from 1 m to 30 m.

OFDM-based UOWC system with a high peak-to-average power ratio (PAPR) is sensitive to the nonlinearity of the LEDs, which is the main reason for out-of-band power and in-band distortion leading to the system performance deterioration. Different approaches have been proposed and implemented for reducing the high PAPR of OFDM signals such as amplitude clipping and filtering, peak windowing, peak cancellation, peak reduction carrier, envelope scaling, decision-aided reconstruction (DAR), coding, partial transmit sequence (PTS), selective mapping (SLM), interleaving, tone reservation (TR), tone injection (TI), active constellation extension (ACE), clustered OFDM, and pilot symbol assisted (PA) modulation [15], [16]. For instance, in [17] a pilot-aided technique was proposed for PAPR reduction of the optical OFDM system, and results showed a 1 dB improvement in the energy-to-noise ratio ($E_{b(opt)}/N_0$) compared to the basic DCO-OFDM at a target BER of 10^{-3}. In [18] the combination of the signal-to-clipping noise ratio (SCR) and the least-squares approximation (LSA) method as a tone reservation scheme was suggested to reduce the PAPR of the DCO-OFDM in an indoor visible light communication (VLC) system. The proposed scheme exhibited PAPR improvement of about 4 dB compared with the original OFDM signal. In [19], a PAPR analysis was carried out for different types of optical OFDM schemes including DCO-OFDM, ACO-OFDM, pulse amplitude modulated discrete multitone (PAM-DMT), and Flip-OFDM. In [20], an OFDM PAPR reduction scheme based on time-frequency domain interleaved was utilized in a UOWC system, which showed a reduction of 8.4 dB in PAPR compared with the original OFDM system. In [21] the repeated clipping and filtering (RCF) method in the frequency domain was used for PAPR reduction and the results confirmed that the RCF method could lead to a reduced overall peak regrowth.

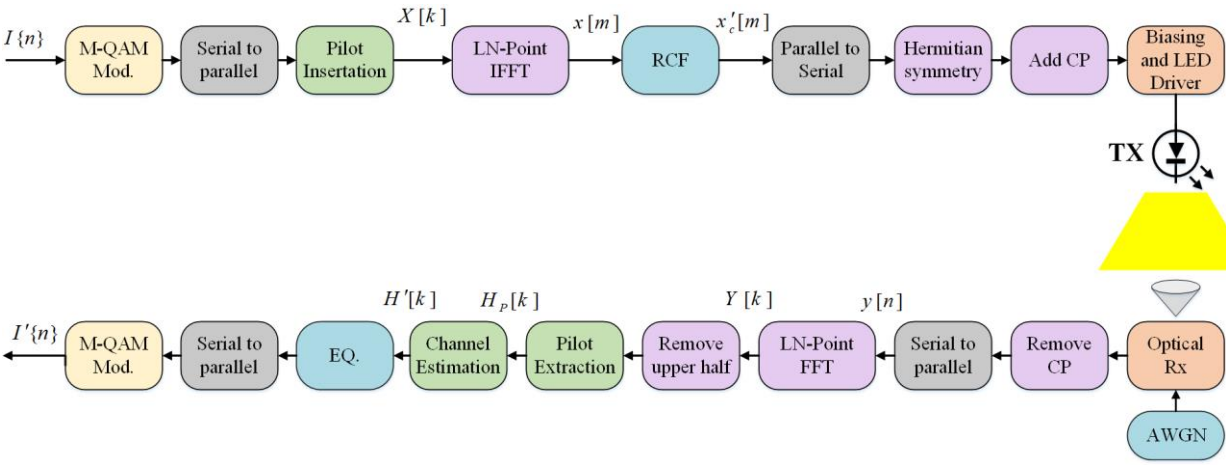

Fig. 1: Schematic block diagram of the proposed DCO-OFDM UOWC system with RCF method.

To the best of the authors' knowledge, the RCF method has not been deeply investigated in the area of UOWC. In this paper, performance of the DCO- OFDM UOWC system is evaluated for two different depths. The minimum mean squared error frequency domain equalizer (MMSE-FDE) is used for channel compensation along with the RCF method to reduce the PAPR. The rest of the paper is organized as follows. In Section 2, an overview of the DCO-OFDM UOWC system with the RCF method including the transmitter (Tx), channel, and receiver (Rx) is explained. In Section 3, the most important results are presented and discussed. Finally, Section 4 concludes the paper.

System Overview

Fig. 1 illustrates the schematic block diagram of the proposed DCO-OFDM UOWC system the with RCF method which is explained comprehensively as follows. The goal is to compare its performance with the DCO-OFDM system without the RCF method under the same conditions.

A. Transmitter

At the Tx, a random data bit stream $\{I_n\}$ is mapped onto the QAM format. Then, the modulated symbols are applied to the serial to parallel (S/P) converter. The pilot insertion block is considered to provide channel estimation at the Rx. Then, the signal is extended by inserting $N(L-1)$ zeros in its middle, resulting in the trigonometric interpolation of the time domain signal, where L is the oversampling factor [22]. The over-sampled signal is passed through an LN-point inverse fast transform (IFFT) block generating the oversampled time-domain OFDM signal followed by the parallel to serial (P/S) converter, which is represented as:

$$x[n] = \frac{1}{\sqrt{LN}} \sum_{0}^{LN-1} X[k] e^{j\frac{2\pi k \Delta f\, n}{LN}} \qquad n = 0, 1, \ldots, LN\text{-}1, \quad (1)$$

As a result of intensity modulation/direct detection (IM/DD), the transmitted signal must be non-negative and real. Therefore, the Hermitian symmetry constraint is imposed to acquire a real-valued signal, as given by [23]:

$$\bar{x}_{HS} = [0, x_{CF}[1], x_{CF}[2], \ldots, x_{CF}\left[\frac{LN}{2} - 1\right], 0, x_{CF}^{*}\left[\frac{LN}{2}1\right], \ldots, x_{CF}^{*}[2], x_{CF}^{*}[1]\,] \quad (2)$$

where $(.)^*$ is the complex conjugate.

A cyclic prefix (CP) is then prepended to each OFDM signal for eliminating the ISI and inter-block interactions (IBI) [12]. Following scaling of the CP added signal $x_{CP}[n]$, we have:

$$I_s[n] = \lambda_s \times x_{CP}[n], \quad (3)$$

where the scaling factor λ_s due to the limited dynamic range of the LED is defined as [24]:

$$\lambda_s = \frac{MI \times I_{max}}{(MI+1)\times \max(x_{CP}[n])}, \quad (4)$$

Here $I_{max} = I_b + 0.5\, I_{PP}$ is the maximum value of I_{in}, I_b is the DC-bias current, I_{PP} is the peak-to-peak current, and MI is the modulation index, which is defined as:

$$MI = \frac{I_{PP} - I_{PP}}{I_b}, \quad (5)$$

Then, following the digital to analog converter, a direct current (DC)-bias I_b is added to the time domain (TD) discrete scaled signal $I_s[n]$ to make it non-negative prior to IM of the light source and transmission over the underwater channel as follows:

$$I_{in}(t) = I_s(t) + I_b, \quad (6)$$

At last, it is fed to drive the LED by convolving with the LED impulse response which is characterized as a first-order low pass Butterworth filter, given by [24]:

$$h_{LED}[n] = \exp[-2\pi f_{LED} n], \quad (7)$$

where f_{LED} is the 3-dB cut-off frequency of the LED. Note, the PAPR is calculated from the L-times oversampled TD signal samples $x[m]$ as [19]:

$$PAPR\{x[m]\} = \frac{max_{0\le t \le NL-1} |x[m]|^2}{E\,[|x[m]|^2\,]}, \quad (8)$$

where $E\{.\}$ is the expectation operator. The complementary cumulative distribution function (CCDF), defined as CCDF ($PAPR$) = P $\{PAPR > PAPR_0\}$, is utilized to appraise the PAPR reduction performance. The target value of PAPR is designated as $PAPR_0$ [20].

B. Channel

Channel modeling plays an important role in the quality evaluation of communication links. A practical and widely used method for modeling the underwater channel is Monte Carlo (MC) simulation to solve the *radiative transfer equation* (RTE). The MC numerical method evaluates the channel characteristics by generating *N* photons through the water simultaneously and then tracking the interactions of each photon with the medium and its trajectory through the channel from the Tx to the Rx. This method is a more flexible and simpler approach without restrictions on the scattering angles compared with the other analytical methods [25].

Three basic attributes of emitted photons include photon's weight, position in Cartesian coordinates (*x*, *y*, *z*), and transmission direction (characterized by polar θ and azimuthal angle φ). Photons interacting with particles in the water experience a change of direction and loss due to both scattering and absorption which can be evaluated by absorption coefficient, $a(\lambda)$, and scattering coefficient, $b(\lambda)$, respectively. The basic rules of this approach are summarized as follows [26], [27]. The initial photon's position is equal to the Tx position which is considered (0, 0, 0) in this study. The angle of θ and φ are chosen randomly between [- θ_{max}, θ_{max}] and

[0, 2π] with uniform distributions, respectively, where θ_{max} is the maximum initial divergence angle. The direction vector (μ_x, μ_y, μ_z) for each photon is equal to $(\sin\theta\cos\varphi, \sin\theta\sin\varphi, \cos\theta)$.

The scattering coefficient is considered to study the effect of multiple scattering which is defined by the integral of the spectral volume scattering function (VSF) over all directions as:

$$b(\lambda) = \int_0^{4\pi} \beta(\theta,\lambda)\, d\Omega = 2\pi \int_0^{\pi} \beta(\theta,\lambda)\, \sin\theta\, d\theta, \quad (9)$$

where $\beta(\theta,\lambda)$ is the VSF and $d\Omega$ is the solid angle centered on θ. Finally, the whole attenuation coefficient of spectral light beam is defined as, $c(\lambda) = a(\lambda) + b(\lambda)$. Note, a,b, and c are in units of m^{-1}. In addition, the angular probability distribution of the scattered photons at a given wavelength, known as the scattering phase function (SPF), is given by:

$$\tilde{\beta}(\theta,\lambda) = \frac{\beta(\theta,\lambda)}{b(\lambda)}, \quad (10)$$

Typically, the Henyey-Greenstein (HG) phase function is used to describe the SPF of dispersive medium such as water and atmosphere with the expression as:

$$\tilde{\beta}(\theta) = \frac{1-g^2}{4\pi(1+g^2-2g\cos\theta)^{3/2}}, \quad (11)$$

where g is the average cosine of θ in all scattering directions and almost equals 0.924 for all water types. At first and before any interactions, the photon passes a certain distance called the step size (Δs):

$$\Delta s = -\frac{\log \xi^s}{c(\lambda)}, \quad (12)$$

where ξ^s is a uniform random variable between [0,1]. After that, the new coordinates of the photon's position are updated according to:

$$\acute{x} = x + \mu_x \Delta s, \acute{y} = y + \mu_y \Delta s, \acute{z} = z + \mu_z \Delta s, \quad (13)$$

The interaction of the photon with the scattering point leads to energy loss and deviation of the photon from the transmission direction. Therefore, the photon's energy level (weight) is updated by:

$$W_{Post} = \left(1 - \frac{b}{c}\right) W_{Pre}, \quad (14)$$

where W_{Post} and W_{Pre} represent the weights after and before the interaction, respectively. The new azimuth ($\acute{\varphi}$) and elevation ($\acute{\theta}$) angles also need to be calculated due to changing the photon transmission direction after the scattering point, as follows:

$$R = 2\pi \int_0^{\acute{\theta}} \tilde{\beta}(\theta) \sin\theta\, d\theta, \quad (15)$$

$$\acute{\varphi} = 2\pi R, \quad (16)$$

where R is a uniform random variable between [0, 1]. Then, from (15), $\acute{\theta}$ can be obtained as:

$$\cos\acute{\theta} = \frac{1}{2g}\left[1 + g^2 - \left(\frac{1-g^2}{1-g+2gR}\right)^2\right]. \quad (17)$$

Finally, the new transmission direction vector can be calculated as [26]:

$$\acute{\mu_x} = -\mu_y \sin\acute{\theta}\cos\acute{\varphi} + \mu_x(\cos\acute{\theta} + \sin\acute{\theta}\sin\acute{\varphi}),$$
$$\acute{\mu_y} = -\mu_x \sin\acute{\theta}\cos\acute{\varphi} + \mu_y(\cos\acute{\theta} + \sin\acute{\theta}\sin\acute{\varphi}),$$
$$\acute{\mu_z} = -\left(\mu_x{}^2 + \mu_y{}^2\right)\sin\acute{\theta}\sin\acute{\varphi}/\mu_z + \mu_z\cos\acute{\theta}, \quad (18)$$

At the Rx side, a photon can be detected when its position and the arrival angle are within the Rx's aperture and Field of View (FOV) and its weight is higher than the threshold level. The process of photon scattering continues until the photon is received at the PD or disappeared by losing all its weight. The threshold weight at the PD is assumed 10^6 in this study.

C. Receiver

At the Rx side, the received signal is detected by an optical Rx composed of a single PD and a trans-impedance amplifier (TIA). The regenerated electrical received signal is given by:

$$y(t) = s(t) * h_c(t) + n(t), \quad (19)$$

where $n(t)$ is the additive white Gaussian noise with the power $P_n = N_0 B_{\mathrm{Rx}}$, N_0 is the noise power. Note, spectral density, and B_{Rx} is the bandwidth of the Rx. $n(t)$ is mostly dominated by the ambient light induced shot noise. Then, the received signal is amplified and converted to a parallel signal via the S/P block. Following CP removal, an N-point FFT block is employed to transform the TD signal $y[n]$ to the Frequency Domain (FD) signal $Y[k]$. The upper half of the signal is removed due to the use of Hermitian symmetry at the Tx side and then the least square (LS) method is utilized to calculate the complex-valued channel frequency response (CFR) based on pilot symbols, as follows:

$$H_p(m) = \frac{Y_p(m)}{X_p(m)}, \qquad m = 1, \ldots, N_p \quad (20)$$

where m is the number of pilot sub-carrier, N_p is the number of pilots in one OFDM symbol, $Y_p(m)$ is the received pilot symbol that are extracted from every eight subcarriers of the received OFDM signal, and $X_p(m)$ is the transmitted pilot symbol. Then, linear interpolation is performed to compute the CFR function on the remaining subcarriers as:

$$\widehat{H}[(m-1)L + \ell] = H_p(m) + \frac{1}{L}[H_p(m+1) - H_p(m)], \quad \ell = 1, \ldots, L \quad (21)$$

where L = 8 is the distance in subcarriers between two consecutive pilots.

A one-tap frequency-domain equalizer (FDE) with the minimum mean square error (MMSE) method is used to compensate for the channel deficiencies. The MMSE coefficients are calculated as follows:

$$C_k^{MMSE} = \frac{\hat{H}_k^*}{\hat{H}_k \hat{H}_k^* + 1/\gamma}, \quad (22)$$

where k is the number of subcarriers, and γ is the signal to noise ratio (SNR). So, the decision variable is calculated as:

$$\hat{S}_k = C_k^{MMSE}\, Y[k]\,, \tag{23}$$

Finally, $\hat{S}_k$ is converted to a serial data stream using a parallel-serial (P/S) block prior to QAM demodulation [28].

D. RCF Method

Fig. 2 illustrates the schematic block diagram of the RCF method. To avoid large PAPR, the clipping technique as a hard limiter is applied to the amplitude of the complex values of the IFFT output. Following, the filtering technique is designed to alleviate or cancel Out of Band (OOB) distortion dependent on the oversampling value however, however it cannot correct in-band distortion.

Fig. 2: Block diagram of the RCF method.

The so-called Repetitive Clipping and Filtering (RCF) is only applied at the Tx end of the OFDM system, however it influences the performance of the Rx signal at the receive end. The RCF algorithm proceeds in four steps [29], [30]:

Step 1: The amplitude of L-times oversampled time domain signal $x[m]$ is clipped while its phase remains unchanged:

$$x_c[m] = \begin{cases} A & |x[m]| < A \\ x[m] & |x[m]| \geq A \end{cases} \tag{24}$$

where A is the threshold clipping level that equals to:

$$A = CR \times \sigma \tag{25}$$

where CR and σ are the clipping ratio and root mean squared value (RMS) of $x[m]$, respectively.

Step 2: The clipping is followed by the FD filtering to reduce OOB distortion caused by clipping. Hence, the clipped TD signal $x_c[m]$ is passed through a filter consisting of FFT and IFFT operators. First, $x_c[m]$ is converted back into the discrete FD as $X_c[k]$ using an FFT. Then, the OOB components of $X_c[k]$ are set to zero while the in-band components are left unchanged. The resultant signal is as follows:

$$\acute{X}_c[k] = [\ X_c[0], \dots, X_c[\tfrac{N}{2} - 1],\ 0,\ \dots,\ 0,\ X_c\left[NL - \tfrac{N}{2} + 1\right], \dots, X_c[NL-1]]\,, \tag{26}$$

Step 3: Then, $\acute{X}_c[k]$ is converted into the TD using the LN-point IFFT block.

Step 4: The filtering technique can lead to peak regrowth. So, repeat K times step 1 to step 3, where K is a positive integer usually chosen between one and four until the amplitude of the OFDM signal is set to a specified threshold level [20].

Result and Discussion

In this section, we present computer simulation results for the proposed system, which are obtained using MATLAB and real-world parameters. All simulation parameters are given in Table 1.

Table 1: System parameters

Symbol	Parameter	Value
-	Modulation type	QAM
$\boldsymbol{M}$	Modulation order	4
$\boldsymbol{N}$	(I)FFT size	256, 1024
-	Pilot type	Comb
$\boldsymbol{N_P}$	Number of pilots	30 (N = 256), 114 (N = 1024)
$\boldsymbol{N_a}$	Number of active subcarriers	224 (N = 256), 910 (N = 1024)
$\boldsymbol{R_b}$	Bit rate (Mbps)	6
$\boldsymbol{N_{CP}}$	Cyclic prefix length	$N/4$
$\boldsymbol{f_{LED}}$	LED cut-off frequency (MHz)	3
$\boldsymbol{\theta}$	LED divergence angle	60°
$\boldsymbol{FOV}$	PD field of view	60°
$\boldsymbol{W_s}$	Signal bandwidth (MHz)	3
$\boldsymbol{f_s}$	Sampling frequency (MHz)	12
$\boldsymbol{\Delta x}$		1 m
$\boldsymbol{L}$	Clipping ratio	4
CR		0.4 :0.2: 4

In Fig. 3, the CCDF function is used to evaluate the PAPR performance of 4-QAM DCO OFDM UOWC system with RCF method for a range of Clipping Ratio (CR) values. The clipping and filtering level, depth, and the number of subcarriers is one, 5 m, and 1024, respectively. The CCDF of PAPR is defined as CCDF (PAPR) = P (PAPR, respectively > $PAPR_0$) where $PAPR_0$ is the target PAPR value. It is clearly shown that utilizing the RCF method leads to the PAPR reduction up to ~4 dB, at CCDF of 10^{-2} and CR =4 compared with the original signal. In addition, it can be seen that the CCDF of PAPR can be remarkably reduced by decreasing CR. The best PAPR reduction is achieved for the lowest CR = 0.4 which is 6.9 and 7.35 dB at CCDF = 10^{-2} and CCDF = 10^{-3}, respectively, compared with the original signal. In fact,

the PAPR performance of the proposed system becomes worse as the CR value increases due to a decrease in the A value which is equal to CR×σ.

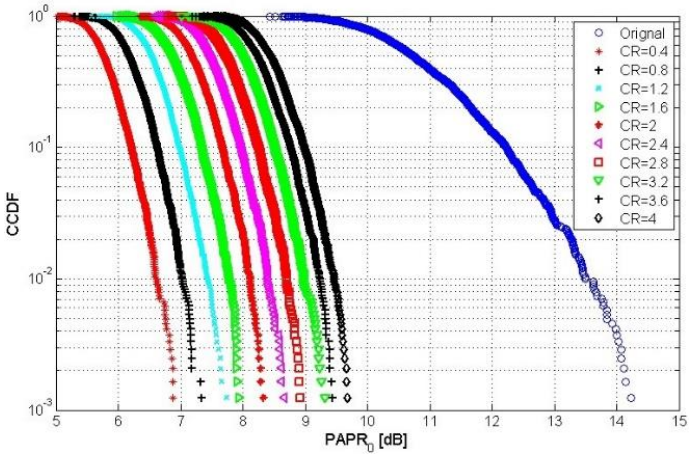

Fig. 3: CCDF performance of the proposed system for one time clipping and filtering and various CR values.

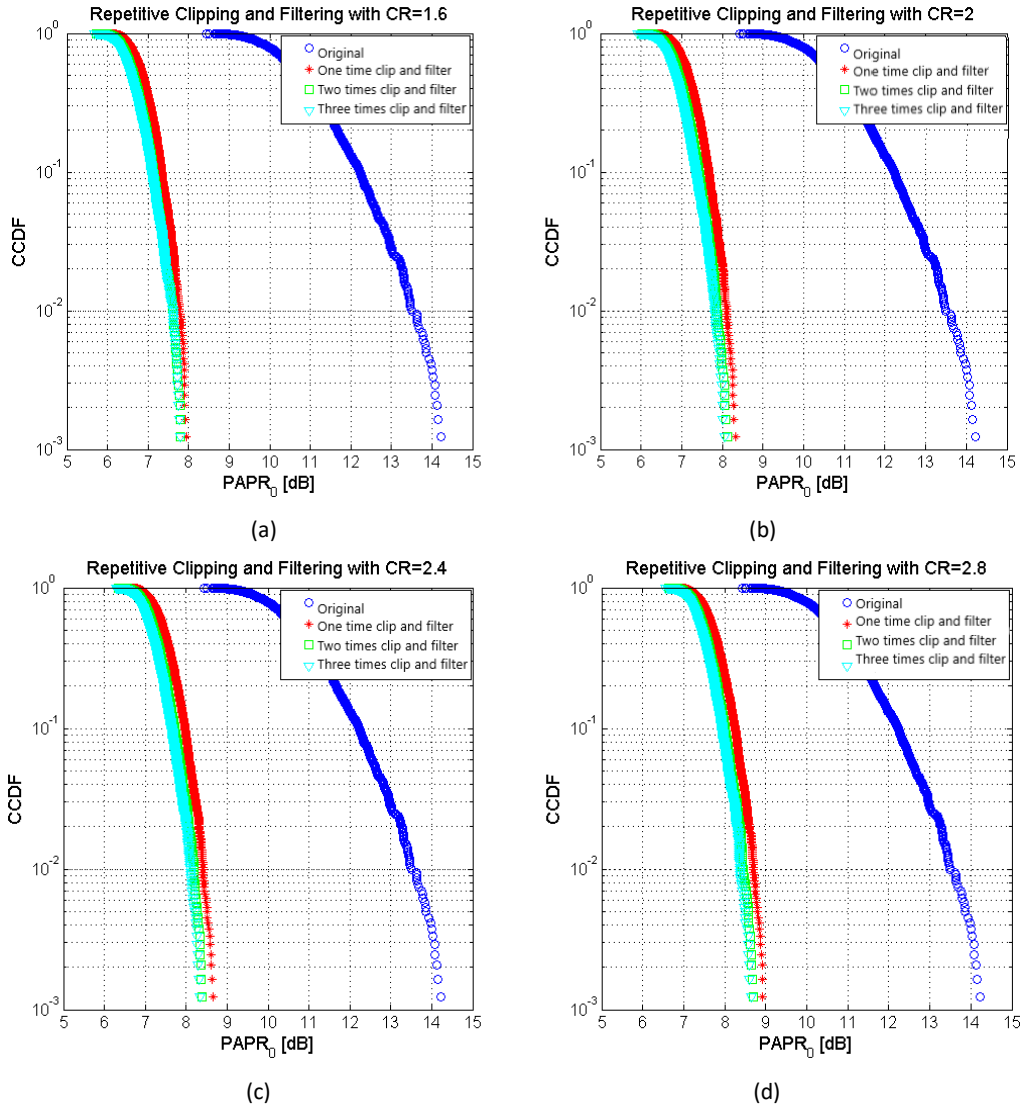

Fig. 4: The CCDF performance of the RCF: (a) CR=1.6, (b) CR=2, (c) CR=2.4 and (d) CR=2.8.

The CCDF performance is also examined when the clipping and filtering levels are 2 and 3 times at the CR of 1.6, 2, 2.4, and 2.8, as shown in Fig. 4. For example, for three times clipping and filtering scenario, the results demonstrate that at CCDF of 10^{-2}, the PAPR gains for the CR = 1.6, 2, 2.4, 2.8 are equal to 7.60, 7.85, 8.19, and 8.41 dB, respectively.

The system BER and EVM performances are also evaluated for different CRs in a 4-QAM DCO OFDM system using RCF method.

As can be seen in Fig. 5, by increasing the gain of CRs both BER and EVM performances of the system are improved.

For instance, CRs of 4, 3.2, 2.8 and 2.4 reach the target BER about 10^{-4} at E_b/N_0 of 13, 14, 16 and 22, respectively.

Next, the performance of the DCO-OFDM UOWC system with and without the RCF method is assessed while two different link lengths of 1 m and 5 m are considered.

As can be seen clearly in Fig. 6 (a), employing RCF method with CR = 3.6 results in improved BER performance up to 10 dB compared with the system without RCF method at target BER = 10^{-4}. In addition, by increasing the link length to 5 m, the proposed method with CR of 3.6 reached the target BER of 10^{-4} at E_b/N_0 of 16 dB.

Finally, we examined the effect of the RCF method on the error floor.

According to Fig. 7, utilizing the RCF method with higher CR at both depths of 1 m and 10 m leads to error floor at low BER values.

In summary, the CCDF of PAPR can be remarkably reduced by decreasing CR. Clearly, utilizing the RCF method leads to the PAPR reduction up to ~4 dB. In addition, the CCDF performance is increased by the number of clipping and filtering iterations, however the improvement is not significant for more than once as evidenced by Fig. 4.

To conclude, clipping and filtering techniques eliminate the out-of-band radiation by clipping the time-domain signal to a predefined level and subsequently filtering.

The relatively small in-band distortion is combatted using low-order signal constellation, coding, and/or clipping noise cancellation techniques, where we have not considered all these techniques in this research. To suppress peak regrowth due to filtering, RCF techniques can be used.

Their convergence rate decreases significantly after the first few iterations. Also, the increased number of iterations leads to increased computational complexity, especially when the number of subcarriers is very large. The convergence rate can be improved by setting the clipping threshold to a level slightly lower than the required level.

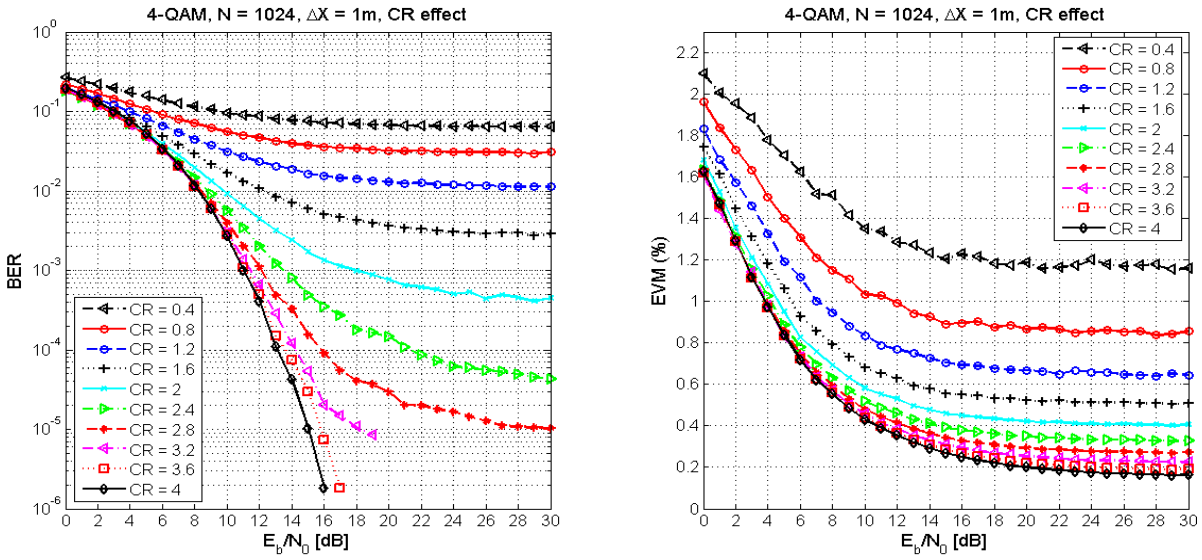

(a) (b)

Fig. 5: BER and EVM vs. E_b/N_0: (a) BER performance and (b) EVM performance.

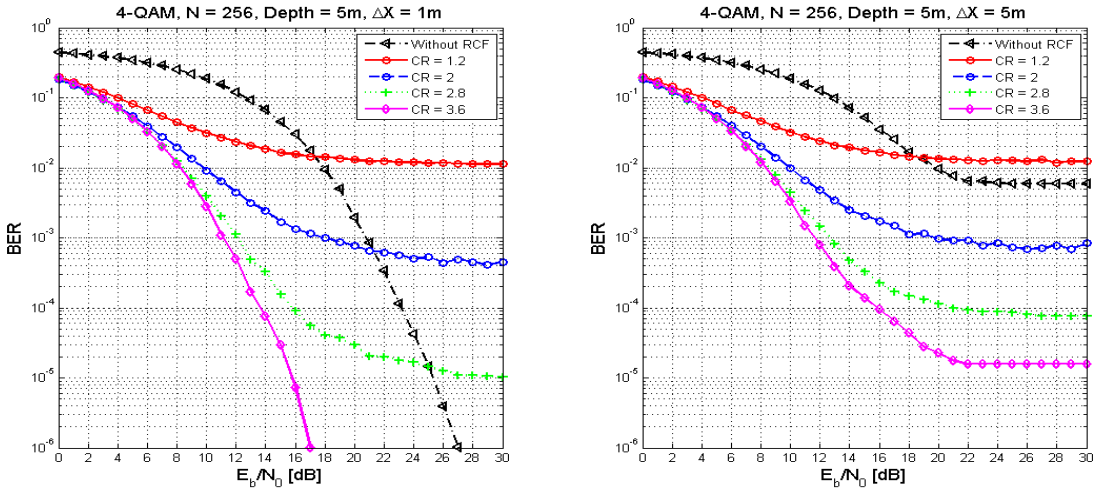

(a) (b)

Fig. 6: BER Performance of the DCO OFDM UOWC system with and without RCF Method: (a) ΔX = 1 m and (b) ΔX = 5 m.

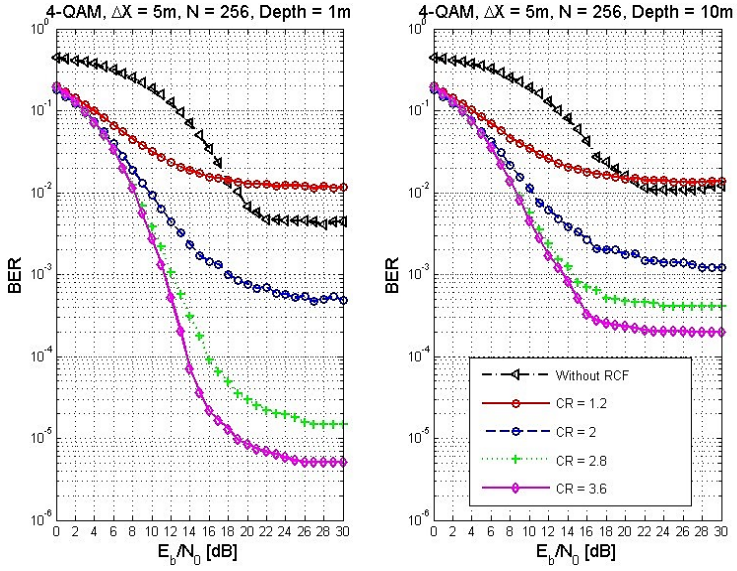

(a) (b)

Fig. 7: The effect of the RCF method on the error floor: (a) depth=1m, (b) depth=10.

Conclusion

In this article the performance of the DCO-OFDM-based UWOC system was evaluated. The MCML method with the HG model of the SPF is employed for channel modeling. The results showed that the system performance is limited by increasing the link length, the number of subcarriers, and depth. Also, the RCF method was successfully utilized to reduce the PAPR of the DCO-OFDM UWOC system and improve BER performance so that the reduced PAPR for CR=4 as the extreme case for CCDF values of 10^{-2} and 10^{-3} are 9.51 dB and 9.72 dB, respectively. It was also shown that by decreasing the CR, the PAPR is reduced at the cost of the BER and EVM degradation. To reduce PAPR even more, other techniques such as multiple signal representation, coding, and Discrete Fourier Transform (DFT) precoding with RCF may be used, which are of our future subject for research.

Author Contributions

All the Authors contributed to all part of preparing and writing of this paper.

Acknowledgment

The author would like to thank the editor and reviewers for their helpful comments.

Conflict of Interest

The authors declare no potential conflict of interest regarding the publication of this work. In addition, the ethical issues including plagiarism, informed consent, misconduct, data fabrication and, or falsification, double publication and, or submission, and redundancy have been completely witnessed by the authors.

Abbreviations

UWC	Underwater Wireless Communications

ROV	Remotely Operated Vehicles
RF	Radio Frequency
ACO-OFDM	Asymmetrically Clipped Optical OFDM
DCO-OFDM	DC-biased Optical OFDM
UOWC	Underwater Optical Wireless Communications
ISI	Inter Symbol Interference
MIMO	Multiple Input- Multiple Output
OOK	On-Off Keying
OFDM	Orthogonal Frequency Division Multiplexing
PAPR	Peak-to-Average Power Ratio
VLC	Visible light Communication
RCF	Repeated Clipping and Filtering
IM/DD	Intensity Modulation/Direct Detection
MC	Monte Carlo
FOV	Field of View
TIA	Trans-Impedance Amplifier

References

[1] S. Hessien, S. C. Tokgoz, N. Anous, A. Boyacı, M. Abdallah, K. A. Qaraqe, "Experimental evaluation of ofdm-based underwater visible light communication system," IEEE Photonics J., 10(5), 2018.

[2] G. S. Spagnolo, L. Cozzella, F. Leccese, "Underwater optical wireless communications: Overview," Sensors, 20(8): 1-14, 2020.

[3] M. F. Ali, D. N. K. Jayakody, Y. Li, "Recent trends in underwater visible light communication (UVLC) systems," IEEE Access, 10: 22169 – 22225, 2016.

[4] I. N'doye, D. Zhang, M. S. Alouini, T. M. Laleg-Kirati, "Establishing and maintaining a reliable optical wireless communication in underwater environment," IEEE Access, 9: 62519 – 62531, 2021.

[5] H. Kaushal, G. Kaddoum, "Underwater optical wireless communication," IEEE Access, 4: 1518 – 1547, 2016.

[6] Z. Zeng, S. Fu, H. Zhang, Y. Dong, J. Cheng, "A survey of underwater optical wireless communications," IEEE Commun. Surv. Tutorials, 19(1): 204-238, 2017.

[7] S. Zhu, X. Chen, X. Liu, G. Zhang, P. Tian, "Recent progress in and perspectives of underwater wireless optical communication," Prog. Quantum Electron., 73: 100274, 2020.

[8] K. Mamatha, K. B. N. S. K. Chaitanya, S. Kumar, A. Arockia Bazil Raj, "Underwater wireless optical communication - A review," presented at the Int. Conf. Smart Generation Computing, Communication and Networking (SMART GENCON), Pune, India, 2021.

[9] N. Saeed, A. Celik, Tareq Y. Al-Naffouri, M. S. Alouini, "Underwater optical wireless communications, networking, and localization: A survey," Ad Hoc Networks, 94, 2019.

[10] J. Xu, A. Lin, X. Yu, Y. Song, M. Kong, F. Qu, J. Han, W. Jia, N. Deng, "Underwater laser communication using an OFDM-modulated 520-nm laser diode," IEEE Photonics Technol. Lett., 28(20): 2133-2136, 2016.

[11] J. Xu, M. Kong, A. Lin, Y. Song, X. Yu, F. Qu, J. Han, N. Deng, "OFDM-based broadband underwater wireless optical communication system using a compact blue LED," Opt. Commun., 369: 100-105, 2016.

[12] R. Kraemer, J. S. Tavares, F. Pereira, H. M. Salgado, L. M. Pessoa, "5.36 Gbit/s OFDM optical wireless communication link over the underwater channel," presented at the 12th Int. Symposium on Communication Systems, Networks and Digital Signal Processing (CSNDSP), Porto, Portugal, 2020.

[13] N. J. Jihad, S. M. Abdul Satar, "Performance study of ACO-OFDM and DCO OFDM in optical camera communication system," presented at 2nd Al-Noor International Conference for Science and Technology (NICST), Baku, Azerbaijan, 2020.

[14] B. Noursabbaghi, G. Baghersalimi, O. Mohammadian, "Performance evaluation of an OFDM-based underwater wireless optical communication depth by considering depth-dependent variations in attenuation," presented at 2nd West Asian Colloquium on Optical Wireless Communications (WACOWC), Tehran, Iran, 2019.

[15] A. Nayak, A. Goen, "A review on PAPR reduction techniques in OFDM system," Int. J. Adv. Res. Electr. Electron. Instrum. Eng., 5 (4): 2767-2772, 2019.

[16] M. Munjure Mowla, M. Yeakub Ali, R. A. Aoni, "Performance comparison of two clipping based filtering methods for PAPR reduction in OFDM signal," J. Mobile Network Commun. Telematics (IJMNCT), 4(1): 23-34, 2014.

[17] F. B. Offiong, S. Sinanović, W. O. Popoola, "On PAPR reduction in pilot-assisted optical OFDM communication systems," IEEE Access, 5: 8916-8929, 2017.

[18] J. Bai, Y. Li, Y. Yi, W. Cheng, H. Du, "PAPR reduction based on tone reservation scheme for DCO-OFDM indoor visible light communications," Opt. Express, 25(20): 24630-24638, 2017.

[19] J. Wang, Y. Xu, X. Ling, R. Zhang, Z. Ding, C. Zhao, "PAPR analysis for OFDM visible light communication," Opt. Express, 24(24): 27457-27474, 2018.

[20] J. Bai, C. Cao, Y. Yang, F. Zhao, X. Xin, A. H. Soliman, J. Gong, "Peak-to-average power ratio reduction for DCO-OFDM underwater optical wireless communication system based on an interleaving technique," Opt. Eng., 57(8), 2018.

[21] J. Armstrong, "Peak-to-average power reduction for OFDM by repeated clipping and frequency domain filtering," Electron. Lett., 38(5): 246-247, 2002.

[22] J. Bai, Y. Li, W. Cheng, Y. Yang, Z. Dua, Ya. Wang, "PAPR reduction for IM/DD-OFDM signals in underwater wireless optical," presented at the 13th IEEE Conference on Industrial Electronics and Applications (ICIEA), Wuhan, China, 2018.

[23] T. Essalih, M. A. Khalighi, S. Hranilovic, H. Akhouayri, "Optical OFDM for SiPM-Based underwater optical wireless communication links," Sensors, 20(21), 2020.

[24] M. Nassiri, G. Baghersalimi, Z. Ghassemlooy, "Optical OFDM based on the fractional Fourier transform for an indoor VLC system," OSA, 60(9): 2664-2671, 2021.

[25] C. Gabriel, M. A. Khalighi, S. Bourennane, "Monte Carlo-based channel characterization for underwater optical communication systems," J. Opt. Commun. Networking, 5(1): 1-12, 2013.

[26] D. Chen, C. Li, Z. Xu, "Performance evaluation of OOK and system based on APD receiver," presented at the 16th Int. Conf. on Optical Communications and Networks (ICOCN): 1-3, 2017.

[27] S. K. Sahu, P. Shanmugam, "A theoretical study on the impact of particle scattering on the channel characteristics of underwater optical communication system," Opt. Commun., 40(8): 3-14, 2018.

[28] J. Alkhasraji, C. Tsimenidis, "Coded OFDM over short range underwater optical wireless channels using LED," presented at the Int. Conf. of Oceans, Aberdeen, UK, 2017.

[29] T. Sri Sudha, G. Sasibhushana Rao, "Clipping based PMPR reduction techniques for LTE-OFDM systems," in Proc. Int. Con. on Intelligent Data Communication Technologies and Internet of Things (ICICI): 1023-1031, 2018.

[30] Z. S. Hadi, B. M. Omran, "Peak-to-Average power reduction using repeated frequency domain filtering and clipping in OFDM," Int. J. Comput. Appl., 122(11): 6-10, 2015.

Biographies

Behzad Noursabbaghi received his B.Sc. degree from Chabahar Maritime University and M.Sc. degree from the University of Gilan, Iran, in 2016 and 2019, respectively, all in Electrical Engineering. His research interests are focused on Visible Light Communications and Underwater Wireless Optical Communications.

- Email: behzadnorsabbaghi@yahoo.com
- ORCID: NA
- Web of Science Researcher ID: NA
- Scopus Author ID:NA
- Homepage: NA

Gholamreza Baghersalimi received his B.Sc. degree from the University of Tehran, Iran, M.Sc. degree from Tarbiat Modares University, Iran, and Ph.D. degree from the University of Leeds, UK, all in Electrical Engineering. Now, he is an Associate Professor in the Department of Electrical Engineering, the University of Guilan. His research interests are in the area of fiber-optic communication systems, optical wireless communications especially visible light communications.

- Email: bsalimi@guilan.ac.ir
- ORCID: 0000-0003-1305-1109
- Web of Science Researcher ID: NA
- Scopus Author ID: NA
- Homepage: https://guilan.ac.ir/~bsalimi

Atiyeh Pouralizadeh received her B.Sc. and M.Sc degrees from the University of Guilan, Iran, in 2017 and 2021, respectively, all in Electrical Engineering. Her research interests are focused on Data and Signal processing, Optical Wireless Communications (OWC), Visible Light Communications (VLC), Machine Learning (ML), Deep Learning (DL) techniques and Neural Networks (NNs).

- Email: atiyehpouralizadeh@gmail.com
- ORCID: 0000-0002-7974-2271
- Web of Science Researcher ID: NA
- Scopus Author ID: NA
- Homepage: NA

Ozra Mohammadian Chakhansar received her B.Sc. degree from Mohaghegh Ardabili University and M.Sc. degree from the University of Guilan, Iran, in 2015 and 2019, respectively, all in Electrical Engineering. Her research interests are focused on non-orthogonal multiple-access techniques, random access protocols, orthogonal frequency division multiple-access.

- Email: ozramohammadian@gmail.com
- ORCID: NA
- Web of Science Researcher ID: NA
- Scopus Author ID: NA
- Homepage: NA

How to cite this paper:
B. Noursabbaghi, G. Baghersalimi, A. Pouralizadeh, O. Mohammadian, "PAPR reduction in OFDM UOWC system employing Repetitive Clipping and Filtering (RCF) method," J. Electr. Comput. Eng. Innovations, 11(2): 301-310, 2023.

DOI: 10.22061/jecei.2022.9061.569

URL: https://jecei.sru.ac.ir/article_1818.html